ELSEVIER

Journal of South American Earth Sciences 21 (2006) 252–266

Journal of
South American
Earth Sciences

www.elsevier.com/locate/jsames

The Cobres Plutonic Complex, eastern Puna (NW Argentina): Petrological and structural constraints for Lower Paleozoic magmatism

A. Kirschbaum [a,b,*], F. Hongn [b], N. Menegatti [a]

[a] *Facultad de Ciencias Naturales, Universidad Nacional de Salta, Buenos Aires 177-4400, Salta, Argentina*
[b] *Conicet- Instituto de Bio y Geociencias (IBIGEO), Museo de Ciencias Naturales, Mendoza 2, 4.400, Salta, Argentina*

Received 1 May 2004; accepted 1 February 2006

Abstract

The southern portion of the Cobres Range is studied with an interdisciplinary, petrological–geochemical and structural-cartographic approach. The Cobres Plutonic Complex (CPC) consists of two main plutons, a granodiorite and a monzogranite, as well as small bodies of gabbros, acidic dikes, and episyenite bands. Their mineralogy and geochemistry suggest a comagmatic character for both plutons, which are strongly peraluminous and define a typical calc–alkaline trend. Harker diagrams indicate a fractionated crystallization trend. The REEs have similar patterns for enclaves, granodiorites, monzogranites, aplites, and acidic dikes, also similar to those from the upper crust rocks. Gabbros included in the CPC show geochemical signatures compatible with the mantle. The CPC is syntectonic, though the granodioritic and monzogranitic plutons represent different stages in the tectomagmatic history of the region. The geology of the CPC and its regional framework show characteristics—thermal anomalies, alternation of contractional and extensional deformational events, magmatic rocks with crustal and mantle affiliations, and contemporaneous extensional basins—that indicate intrusion of the CPC in an extensional accretionary orogen.

Keywords: Puna; Granitoids; Lower Paleozoic; Extensional accretionary orogen

1. Introduction

Unraveling the Lower Paleozoic magmatism in the central Andes is one of the keys for interpreting the geological evolution of the northern and central Argentine basement rocks. The latest, most widespread investigations of Eopaleozoic plutonism point mainly to regional syntheses (e.g. Rapela et al., 1998; Coira et al., 1999) on the basis of detailed analysis of individual plutons. Comprehensive studies of single plutons have concentrated mainly on the basement of southern Sierras Pampeanas (e.g. Lira and Kirschbaum, 1990; Rapela et al., 1998). In contrast, detailed investigations of the Paleozoic plutons widely distributed along the basement of the Puna, the northern Sierras Pampeanas, and the Cordillera Oriental remain scarce. Thus, further research is required on Lower Paleozoic plutonism to determine their geological meaning and improve regional syntheses.

Lower Paleozoic magmatism exposed along the eastern border of the Puna (Fig. 1) includes volcanic, subvolcanic, and plutonic manifestations that have been interpreted in the regional and geodynamic syntheses proposed in the past 30 years as follows: a Silurian magmatic belt named Faja Eruptiva de la Puna Oriental, composed of southern plutonic and northern hypabyssal portions (Méndez et al., 1973); Upper Ordovician magmatic arc linked to an east-facing subduction system (Coira et al., 1982); Devonian plutonic belt intruded into an active dextral N–S shear zone (Bahlburg, 1990); plutonic–volcanic belt mainly pre- or syntectonic with an Uppermost Ordovician deformation (Hongn, 1994); and intracontinental magmatic arc linked to oblique contraction–extension (Coira et al., 1999) or oblique contraction (Hongn and Mon, 1999). The plutonic constraints of these interpretations have been based mainly on geochemical data, some structural observations, and regional mapping, but none focused on a detailed study of a single pluton.

Taking into consideration the need for detailed characterizations of the Puna eastern border plutons, an interdisciplinary study, mainly petrologic and structural, was performed on the plutonic rocks of the Cobres Range. This range displays particularly interesting features that help explicate the Lower Paleozoic geological evolution of the Puna region. Specifically, (1) the plutonic rocks are

* Corresponding author. Address: Museo de Ciencias Naturales, Facultad de Ciencias Naturales, Universidad Nacional de Salta, Mendoza 2, 4400, Salta, Argentina.
E-mail address: alikir@unsa.edu.ar (A. Kirschbaum).

0895-9811/$ - see front matter © 2006 Published by Elsevier Ltd.
doi:10.1016/j.jsames.2006.04.003

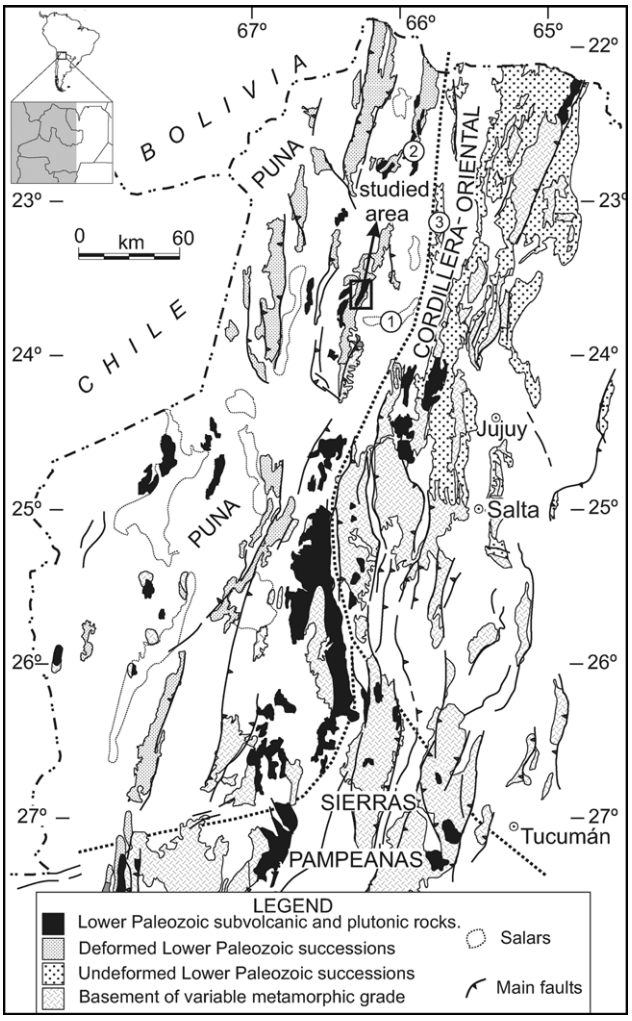

Fig. 1. Map showing the main units of the Neoproterozoic–Lower Paleozoic basement in NW Argentina and the location of the studied area. Numbers identify localities mentioned in text: (1) Salinas Grandes; (2) Cochinoca Range; (3) Aguilar Range.

the easternmost expression of Lower Paleozoic magmatism in the eastern Puna between 23° and 24°SL, (2) the Ordovician host rocks show strong metamorphic transformations linked to the pluton-related thermal anomaly, (3) the Paleozoic deformational and metamorphic fabrics in the Cobres Range permit the establishment of a fairly well-constrained evolution of events, and (4) fossil records in the Ordovician successions distributed around the Cobres Range (Benedetto et al., 2002) and the U/Pb age of plutonic rock in the north portion of the Cobres Range (Lork and Bahlburg, 1993) permit the relationship of absolute and relative temporalities.

This article presents the first results of our petrological work on the Cobres plutonic rocks. Although it describes almost exclusively geochemical and petrological features and their significance in obtaining an accurate interpretation of the plutonic rocks, the final discussion of the magmatic–tectonic evolution of the Cobres Plutonic Complex (CPC) is constrained by hypotheses based on structural analysis. Our results greatly increase knowledge about the geology of the Cobres Range Paleozoic plutonic rocks, and we discuss some interpretations that can be drawn therefrom.

2. Geologic framework

The Cobres Range constitutes a portion of the hills on the eastern border of the Puna, which in turn form the western limit of the Salinas Grandes depression (Fig. 1). It is almost entirely made up of Lower Ordovician (Tremadocian–Arenigian) lithological units, including episodes of sedimentation, metamorphism, magmatism, and deformation. The Cobres Range comprises heights distributed between the Cobres locality to the south and Las Burras River to the north. The map in Fig. 2 shows the geology of the southern half of the range, where our studies concentrated.

The pluton host rock of the Cobres Range corresponds to an alternation of mudstones and sandstones with an intercalation of carbonate levels and seams of polymetallic mineralization (Lurgo Mayón et al., 1999). Quartzite intercalations up to 50 m thick appear toward the upper portions of the section.

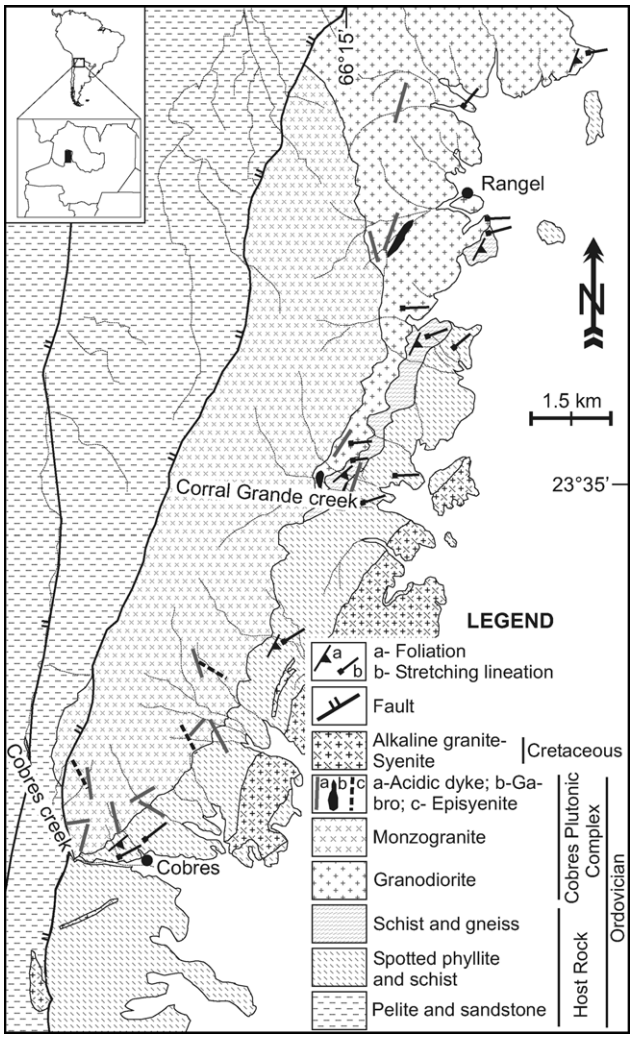

Fig. 2. Geological map of the southern portion of the Cobres Range. Modified from Hongn et al. (2001).

Sedimentary features of the succession (lenticular stratification, cross-bedding associated with wave action, limestone banks, and sandy levels) suggest a platform environment, as previously noted by Lurgo Mayón et al. (1999). There is no fossil register in the Cobres Range metasediments. These rocks may be attributed, with reservation, to the Tremadocian, in view of the fossils found in platform successions a few kilometers to the south (Early Tremadocian, Vaccari et al., 1999) and in turbidites with volcanic intercalations a few kilometers to the east (Late Tremadocian, Benedetto et al., 2002).

Previous investigations of the plutonic rocks from Cobres Range (Zappettini, unpublished) have identified a granodioritic (Lower Paleozoic Cobres granodiorite) and leucogranitic (Upper Paleozoic Bayo leucogranite) pluton. The cartography developed herein indicates the existence of a monzogranitic pluton among the outcrops previously identified as Cobres granodiorite (Fig. 2). Thus, a modification of the stratigraphic nomenclature is necessary; we follow Acuña (unpublished) and include the granodioritic and monzogranitic plutons in the CPC.

The plutons have lithological and structural features that clearly differentiate them, and though they are interpreted as relating to the same Paleozoic magmatic cycle, their origin and emplacement register distinct tectomagmatic evolution stages. The leucogranitic facies are excluded from the CPC, given their Upper Paleozoic age (Zappettini, unpublished) and because their relation to the Ordovician complexes has not been analyzed in detail. However, the first studies carried out on these rocks suggest that they may be part of the CPC; we leave the possibility of their inclusion open.

Other Lower Paleozoic plutons crop out near Las Burras River, northwest of the CPC: Quepente granodiorite, Peladar porphyry, Churcal granite, and Las Burras granite (Zappettini, unpublished). The relationships between these plutons and those cropping out along the Cobres Range are currently being studied.

The CPC host rocks display different metamorphic transformations. Three principal lithological types are defined (Fig. 2) according to features observed in outcrops and thin sections: (1) sandstone and pelite with very low-grade metamorphism (lower greenschist facies), (2) spotted phyllite–schist, and (3) schist and gneiss.

The western portion of the mapped area is dominated by sandstones and pelites, which are in contact with the granodioritic and monzogranitic facies through a reverse fault, except in the Cobres Creek, where they are intruded by the monzogranite. They correspond to a clastic succession affected by very low-grade metamorphism related to the tectonometamorphic event that produced folding with axial plane cleavage. Fine micas (chlorite and white mica) associated with the cleavage constitute the principal mineral growth. Spotted phyllite–schists constitute the most widespread rocks on the eastern border of the range in the mapped area. Monzogranite intrudes this lithology on its eastern and southeastern borders. The spotted rocks show porphyroblasts of 0.2–4 mm; the porphyroblasts overprint the cleavage on the pelitic protoliths. They generally consist of biotite, though chloritic mottles are found in areas further removed from the granodioritic pluton. An incipient metamorphic layering, the increase in grain size, and the disappearance of the sedimentary features mark the transition from spotted facies to schists and gneiss. Porphyroblasts transformed into an aggregate of very fine mica, including possible relicts of cordierite, are visible in the transition between spotted and gneissic facies. The schist and gneiss constitute a belt in contact with the granodiorite, extending between Corral Grande Creek and Rangel village; the belt is truncated by the monzogranite at its southern end. The primary features of the sedimentary rock are totally transposed by tectometamorphic layering, defined by quartzofeldspathic and mica (biotite–muscovite) domains.

The schist and gneiss display levels with cordierite. They are medium- to coarse-grained rocks, registering intense metamorphic segregation with diffusion of the feldspathic material and in certain cases are reminiscent of migmatite.

The phyllite, schist, and gneiss show a well-defined, gently plunging (up to 30°), NE- to E-trending stretching lineation (Fig. 2). Foliation and lineation are characteristic features of these lithologies (Hongn et al., 2001).

Spotted rocks, schist, and gneiss are the result of a high-T metamorphic overprint on pelite and sandstone originally metamorphosed at lower greenschist conditions. The distribution of the high-T metamorphic rocks points to their connection with the granodiorite, because gneiss and schist always show concordant contacts with the granodiorite. The monzogranite cut discordantly the contact between granodiorite and high-T metamorphic rocks at the Corral Grande Creek area (Fig. 2). However, the monzogranite intrudes the granodiorite and metamorphosed (greenschist grade) pelite and sandstone, producing on the most recent a thin metamorphic aureole ($\sim$100 m wide), shown as weak mineralogical and fabric transformations.

Field relationships and fabric overprints suggest the following sequence of events: (1) folding with cleavage at lower greenschist metamorphic conditions; (2) ascent emplacement of granodiorite, high-T metamorphism, and development of high-T deformational fabrics; and (3) ascent emplacement of monzogranite.

3. Cobres Plutonic Complex (CPC)

The CPC extends along the length of the Cobres Range between Las Burras River and Cobres village. The outcrops occupy a surface of approximately 70 km^2. Most of the western border is limited by a fault, whereas the eastern one preserves the original intrusive contact with phyllite, schist, and gneiss. The CPC is elongated in a NNE direction and composed of a monzogranite and a granodiorite, which are clearly distinguishable by their field relations, lithology, petrography, and chemical composition. Acidic dikes (monzodiorite–aplite–pegmatite) and small bodies of gabbro and episyenite strips also form part of the CPC (Fig. 2).

3.1. Field relationships

The granodioritic pluton is mainly composed of grey, inequigranular, medium-grained granodiorites with plagioclase megacrystals of up to 1 cm, which sporadically reach lengths of 3 cm. Scarce tonalites have diffuse contacts with granodiorite on the SE border of the pluton. These are finer-grained rocks that maintain the megacrystals, showing a marked porphyritic texture, and they contain less quartz and more biotite.

The granodiorite includes fragments of gabbro (sample CO-15) in the Corral Grande Creek, which seem related by mingling phenomena. However, the scarce and small gabbro outcrops do not offer more detailed information. Meanwhile, gabbros are considered part of the CPC.

The schist and gneiss always constitute the granodiorite country rock, as also occurs toward the north, in the portion of the CPC not included in Fig. 2. The granodiorite only makes contact with the pelite and sandstone by an east-dipping reverse fault that moves the intrusive over the lower metamorphic grade country rocks. The contact between the granodiorite and the schist–gneiss generally is concordant or subconcordant with the metamorphic foliation; it is sharp or displays a thin zone in which the granodiorite intercalates with the metamorphic rock in dikes parallel to the foliation of the metamorphic rocks.

The northern half of the contact indicated between Corral Grande Creek and Rangel village is a deformation zone with well-defined foliation and lineation. This deformation zone developed at medium to high temperature, according to feldspar recording dynamic recrystallization, undulose extinction, replacement by myrmekites, and the quartz ribbons with incipient development of mosaic or chessboard fabric (Passchier and Trouw, 1996). In addition to the high deformation zone affecting portions of the contact, other medium- to high-temperature deformation zones, with similar foliation and lineation orientation, can be observed in the granodiorite and especially in the host rock (Hongn et al., 2001).

The monzogranitic pluton is homogeneous and porphyritic, with a medium- to coarse-grained matrix containing microcline megacrystals of up to 10 cm but usually 5 cm long. The monzogranite intrudes the granodiorite and the different types of metamorphic rocks. Large granodiorite enclaves within the monzogranite rocks confirm the intrusive sequence.

Although the monzogranite on the whole is concordant with the phyllite and schist foliation, it clearly cuts across the granodiorite and the schist–gneiss strip near Corral Grande Creek, providing evidence of the discordant nature of the intrusion. The intrusive contact of the pluton is principally preserved on the eastern border, with a NNW–SSE-trending portion followed by a segment with NNE-SSW direction (Fig. 2). This geometry suggests a pluton of elliptical primary shape with a NNE–SSW-trending major axis. A small portion of monzogranite, showing the intrusive contact with the weakly metamorphosed sandstones and pelites, is preserved in the footwall of the fault marking the western contact. As mentioned in Section 2, these sandstone and pelite display a thin zone of weakly spotted rocks expressing the contact aureole, which in turn indicates that the greater metamorphism of the eastern monzogranite country rock between Cobres village and Corral Grande Creek is related to the thermal episode associated with the granodiorite. Furthermore, a fabric without preferred orientation overprints the characteristic planar–linear fabric of the schist in the zone in which the transformations related to the monzogranite intrusion appears; therefore, the planar–linear fabric of the metamorphic country rocks precedes the monzogranite intrusion. The absence of high-temperature deformation and the attitude of the low-temperature deformation zones developed in the monzogranite (subvertical foliation striking NW–SE and close to the vertical lineation lying on the foliation) reinforce this hypothesis.

Mafic microgranular enclaves included in the monzogranite show finer grain sizes, diffuse contact with the host rock, and diameters of 3–10 cm.

The CPC includes dikes of different compositions that can be separated into three groups (Fig. 2): (a) acidic, principally aplite and pegmatite; (b) basic; and (c) episyenites. A feature shared by the acidic and episyenite dikes is the predominantly highly dipping NNW–NW alineation. These orientations are subperpendicular to the stretching lineation in the granodiorite and metamorphic host rocks. The basic dike, in contrast, strikes NE.

The aplite–pegmatite dikes, mainly aplites (0.05–2 m thick), are dominant. They register brittle and ductile deformation structures. The former are represented by open fractures parallel to the dike walls and partially filled by druses whose quartz crystals are directed toward the center of the dike. The ductile structures correspond to narrow, low-temperature deformation zones; foliation is parallel to the dike walls and stretching lineation is close to the foliation dip. This ductile deformation does not modify, or weakly modifies, the sharp, planar, and generally parallel contacts of the dikes. Aplites are more frequent in the border areas of the monzogranitic pluton. Where they are placed in the granodiorite or metamorphic rock, they cut the high-temperature, solid-state deformational fabrics discordantly, and they frequently contain quartz–tourmaline veinlets. One monzodioritic dike is included in the acidic dikes.

Basic rocks display different field relationships. In addition to gabbros apparently mingled with the granodiorite, there are also gabbroic and basaltic dikes. The gabbroic dike (sample Cb24a) crops out east of Rangel village with the monzodioritic dike; it is close to 10 m thick and has irregular contacts with the granodiorite. It is described as a dike because the outcrops show its length to be notably greater than its thickness; however, because the quality of the exposures is not good, it may actually be a lenticular gabbroic body.

These gabbro and monzodiorite dikes are cut by a carbonate dike mainly composed of calcite, typical of Cretaceous magmatism (Fig. 2) in the region (Zappettini, unpublished; Menegatti, 2001), which offers an added argument in favor of associating them with the CPC. Gabbroic rocks of this type were not found in the monzogranite.

The basaltic dikes related to Cretaceous magmatism are clearly distinguishable in the field due to the contrast in color

and net sharp contact among them and granitoids. They have planar and parallel borders (thickness 0.5–1.5 m) and porphyritic texture, with plagioclase megacrystals in an aphanitic matrix.

Zappettini (unpublished) indicates the presence of episyenites in the Tusaquillas batholith, NW of Cobres hill, hosted by a two-mica leucogranite. Strips of yellowish to reddish rocks intercalated with the unaltered or less altered monzogranitic crop out on Cobres Range, always associated with brittle deformation zones. They are lentiform-shape bodies, elongated parallel to the deformation zones in the pluton, with mainly transitional or occasionally sharp contacts with the host rock. The episyenites represent postmagmatic hydrothermal phenomena along intensely fractured belts and are described as dikes due to their geometry.

3.2. Age

The age of the CPC is partially constrained by an U/Pb age on monacite from the granodioritic pluton (476 ± 1 Ma, Lork and Bahlburg, 1993). The analyses of the structure and field relationships indicate that the granodiorite is the oldest pluton within the CPC.

There is no absolute age for the monzogranite. However, the hypothesis of its emplacement in spaces generated during the deformation of granodiorite and metamorphic rock (Hongn et al., 2001) points to a younger but similar age for the granodiorite, taking into account that emplacement and high-temperature deformation of the latter are contemporary processes. This hypothesis is consistent with the presence of granodiorite enclaves in the monzogranite.

The geochemical analysis presented next supports the idea that the granodiorite and monzogranite are intrusions intimately related in their origin.

3.3. Petrography

The granodiorites are medium-grained grey rocks, with scarce acidic plagioclase crystals of up to 1 cm long and numerous mafic enclaves. Plagioclase and quartz are the essential minerals, with sparse perthitic microcline. Biotite and tourmaline are the predominant accessories, with smaller proportions of opaque minerals, apatite, zircon, and monazite. Evidence of ductile deformation, such as dynamic recrystallization in quartz or kink bands in biotite, is frequent. A late magmatic alteration process formed the assemblage muscovite + quartz + opaque minerals + chlorite from a primary mafic mineral. This alteration assemblage coexists with primary biotite and tourmaline. Microenclaves with the same mineralogy as the host rock differ only in a greater concentration of mafites.

The monzogranites are medium to coarse grained, porphyritic, and rich in randomly distributed mafic enclaves. They consist of perthitic microcline, plagioclase, and quartz, with accessory minerals similar to the granodiorites. This monzogranite has a greater late tourmaline concentration (hereafter referred to as tourmaline 2 to differentiate it from

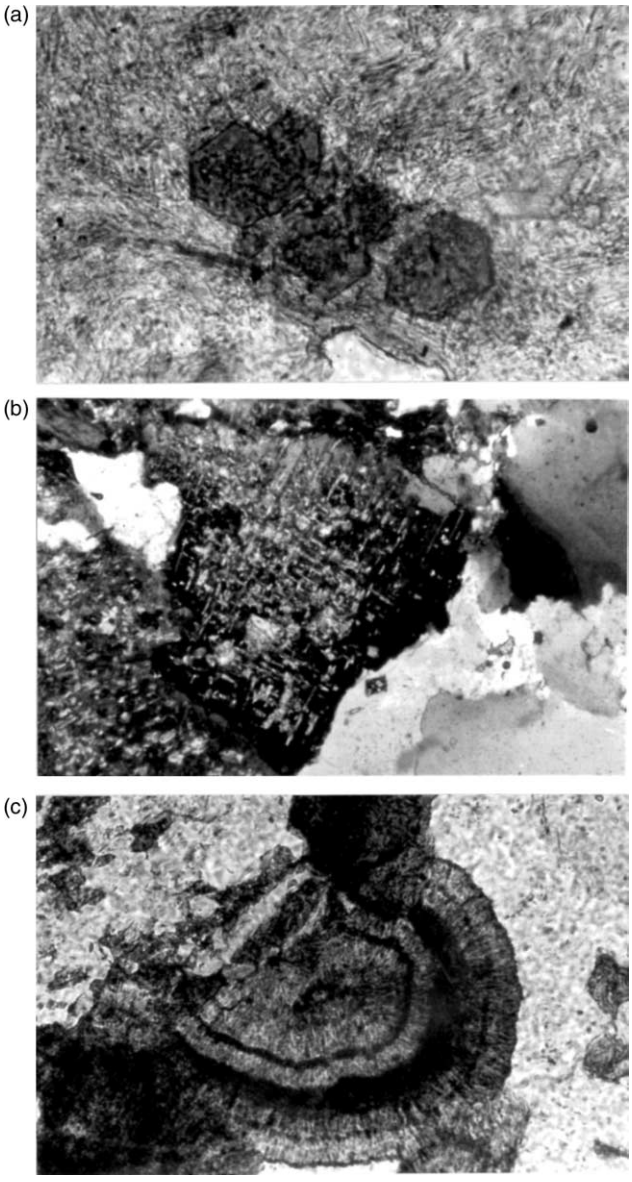

Fig. 3. Mineral associations related to postmagmatic hydrothermal processes: (a) Euhedral sections of schorl in clorithic groundmass (CO-11). (b) Monzogranite with plagioclase transformed into muscovite + quartz + epidote and quartz with crenulated borders (CO-4). (c) Amorphous silica with Fe oxides filling fractures in epysienite (EP-11b). Cross nicols for all.

that which participates with the biotite in the early paragenesis; Fig. 3(a)), particularly associated with the microlitic cavities.

There is a remarkable development of epidote crystals related to deformed rocks and/or intense hydrothermal alteration (Fig. 3(b)), which are accompanied by plagioclase muscovitization and mafite chloritization. Hydrothermal alteration processes are common in all the samples, and some quartz shows weak undulose extinction.

The mafic microgranite possesses a particular texture, in which the plagioclase crystals form a network of cavities within which the quartz crystallized. Their mineralogy is similar to that of the predominant facies, with biotite as the principal mafite and subordinate tourmaline. The accessories

are opaque minerals, zircon, and apatite in small prisms. Reaction processes between mafic enclaves and granodiorite are frequent, with biotite rings around the enclaves. Epidote crystals can be seen in some samples, interpreted as related to hydrothermal processes because they are accompanied by pervasive sericitization, plagioclase muscovitization, and biotite chloritization. Granodioritic enclaves (CB-11b) are identified near the epysienites.

The aplites represent the most evolved rocks within the CPC. They are leucocratic rocks of consertal to migrographic texture, characterized by interdigitations involved in the boundary between crystals, which gives them a notched or serrated appearance. Mineralogically, they are composed of quartz, plagioclase, and perthitic microcline with scarce biotite. Muscovite and schorl are the principal accessories. The biotite shows chloritization and muscovitization.

The monzodioritic dike (sample CB-24c) is made up of andesine (partially transformed into sericite–muscovite) phenocrystals in a matrix formed of microcrystalline quartz, acicular apatite, titanite, allanite, zircon, and tremolite.

The mingled gabbros (sample CO-15) are fine grained and inequigranular, with plagioclase and hornblende as predominant minerals and subordinated opaque minerals, together with chlorite and epidote, as secondary minerals.

Tephrites, trachybasalts, basalts with volcanic textures, gabbros, and lamprophyres constitute the lithology of the dikes related to the Cretaceous magmatism. Mineralogical features separate dikes assigned to the Ordovician plutonism from those emplaced during the Cretaceous magmatism: The former have a simple mineralogy, with hornblende, plagioclase, apatite, opaques, tinanite, and zircon, whereas the Cretaceous bodies show a more complex mineralogy, including plagioclase, sodic ferrohornblende, olivine, barkevikite, clinopyroxene, and titanoilmenite. Strong hydrothermal alteration produced caolinization and sericitization in plagioclases, chloritization of mafites, and the generation of skeletal opaque minerals.

The episyenites are characterized by a decrease in quartz content and cataclastic texture. The primary plagioclase is transformed into an aggregate of fine-grained muscovite and albite. The microcline maintains its optical characteristics, with the alteration centered on the perthitic plagioclase intergrowths, which is totally transformed into muscovite tinted by iron oxides. The primary biotite is replaced by fine-grained, radiated, fibrous in parts, green neo-biotite. Recrystallized quartz occurs in the intercrystalline borders. The episyenitization processes did not affect zircon and apatite. Euhedral rutile crystals also are observed. In some cases, magnetite veins a few centimeters thick are seen in the center of the episyenite strips.

The neominerals present are as follows: (1) euhedral to subhedral albite showing a mosaic texture; (2) large crystals of muscovite I and a network of small muscovite II crystals after the plagioclase; and (3) microcrystalline quartz infilling fractures and crusts of brownish, kidney-shaped amorphous silica (Fig. 3(c)) that precipitated in cavities.

3.4. Postmagmatic processes

The CPC shows hydrothermal alteration mainly concentrated along deformation bands that acted as fluid channel ways. All rocks show the effects of a late hydrothermal front that produced mineralogical and chemical variations, which makes their descriptions necessary.

3.4.1. Pervasive argilization and sericitization

These are frequent in plagioclase, with muscovitization and epidotization in the nuclei (Fig. 3(b)). Plagioclase also shows borders with albitization and recrystallized quartz-filling fractures. The presence of a mafite totally transformed into a sericite + muscovite + chlorite + quartz assemblage, coexisting with biotite and tourmaline, is common in the granodioritic and monzogranitic facies. The hydrothermal processes did not modify apatite, zircon, and monacite optically.

3.4.2. Tourmalinization

There are two types of tourmaline: a primary brownish one associated with biotite and with zircon, apatite, and opaque inclusions and another of hydrothermal origin, associated with the pervasive chloritization and sericitization processes. The latter consists of light blue, subhedral to euhedral crystals without inclusions (Fig. 3(a)).

3.5. Geochemistry

Twenty-six chemical analyses were carried out (Table 1). Some, including the rare earth analyses, were conducted by ICP/MS at Activation Laboratories (Canada) and others by XRF at Universidad Nacional de Salta and Universidad Nacional de Jujuy (Argentina). Three samples from the Cretaceous basic dikes (CB-24a, CB-24b, CO-12) are included in the tables and diagrams to show their chemical variations in comparison with the CPC rocks.

3.5.1. Major and trace elements

Geochemical classification of the rocks is according to diagram R1–R2 (Fig. 4), which shows that the predominant rock types are distributed in the monzogranitic and granodioritic fields, as well as the aplites. The enclaves do not follow the expected trend, in that they are found in the syenitic field due to alkali enrichment produced by the pervasive hydrothermal alteration, shown as sericitization, albitization, and chloritization.

The geochemistry from the gabbroic dike places this rock in the olivine–gabbro field; though olivine is not observed microscopically, the high Cr and Ni concentrations suggest its presence.

The Cobres Range plutons are subalkaline (Fig. 5). The mafic enclaves, because of alkaline enrichment due to late magmatic processes, are distributed in the alkaline field.

The alumina saturation indices (Fig. 6) point to the strongly peraluminous character of the main magmatism, which is coherent with the presence of normative corindon (2.3–4.9%, Table 1) and muscovitization processes. The basic dikes are meta-aluminous, but the monzodioritic dike moves away from

Table 1
Analyses of CPC rocks

Lithology	Monzogranites								Granodiorites				
Sample	CO-0**	CO-4	CO-6	CO-8	CO-11	CO-13	CO-14	CO1-17*	CB-22	CB-28	CB-37	CO-16	CO-17
SiO_2	70.26	69.85	67.57	70.17	69.81	69.52	71.04	73.81	69.21	68.40	68.55	68.75	68.30
TiO_2	0.56	0.49	0.52	0.41	0.48	0.56	0.61	0.06	0.61	0.64	0.61	0.66	0.62
Al_2O_3	14.36	14.00	15.31	13.98	14.30	14.19	14.08	14.76	14.34	15.02	15.21	14.80	14.55
Fe_2O_3	3.73	3.64	3.64	3.21	3.42	4.08	3.80	0.58	4.85	4.80	4.72	4.83	4.63
MnO	0.05	0.04	0.07	0.06	0.06	0.07	0.06	0.01	0.09	0.09	0.07	0.07	0.08
MgO	1.19	1.12	1.20	1.04	1.13	1.35	1.28	0.27	1.97	1.97	1.87	1.98	1.84
CaO	1.32	1.48	1.65	1.19	1.21	1.57	1.34	0.39	1.23	1.52	1.26	1.70	1.47
Na_2O	2.81	2.84	3.22	2.75	2.79	2.75	2.55	3.61	2.42	2.69	2.72	2.29	2.61
K_2O	4.65	4.38	4.76	4.87	5.24	4.10	4.46	5.44	3.93	3.70	4.10	3.32	3.96
P_2O_5	0.20	0.20	0.20	0.20	0.21	0.21	0.20	0.20	0.20	0.19	0.19	0.21	0.19
LOI	1.07	0.77	0.82	0.89	1.02	0.99	0.99	0.72	1.30	1.38	1.12	1.31	1.11
Total	100.20	98.81	98.96	98.77	99.67	99.38	100.41	99.85	100.15	100.39	100.42	99.91	99.35
Q	32.08	32.29	25.86	32.00	29.84	33.05	34.92	31.31	35.08	32.93	32.08	36.72	32.60
C	2.78	2.38	2.34	2.50	2.34	2.88	3.10	2.71	4.35	4.28	4.46	4.85	3.75
Or	27.48	25.89	28.13	28.78	30.97	24.23	26.36	32.15	23.23	21.87	24.23	19.62	23.41
Ab	23.78	24.03	27.24	23.27	23.61	23.27	21.58	30.54	20.48	22.76	23.01	19.38	22.08
An	5.24	6.04	6.88	4.60	4.63	6.42	5.34	0.64	4.80	6.30	5.01	7.06	6.05
Di													
Hy	2.96	2.79	2.99	2.59	2.81	3.36	3.19	0.67	4.91	4.91	4.66	4.93	4.58
Ol													
Hm	3.73	3.64	3.64	3.21	3.42	4.08	3.80	0.58	4.85	4.80	4.72	4.83	4.63
Il	0.11	0.09	0.14	0.13	0.13	0.14	0.14	0.03	0.19	0.19	0.15	0.15	0.16
Tn													
Pf													
Ru	0.50	0.44	0.44	0.34	0.41	0.48	0.54	0.04	0.51	0.54	0.53	0.58	0.53
Ap	0.47	0.47	0.47	0.47	0.50	0.50	0.47	0.46	0.47	0.45	0.45	0.50	0.45
Total	99.13	98.06	98.13	97.89	98.66	98.41	99.44	99.13	98.87	99.03	99.30	98.62	98.24
V	48	59	50	51	50	62	60	–	119	86	79	81	101
Cr	–	–	–	25	–	–	–	6	52	47	51	–	63
Co	–	–	–	33	–	–	–	16	33	30	28	–	39
Ni	–	–	–	nd	–	–	–	nd	28	28	26	–	nd
Cu	–	–	–	nd	–	–	–	–	35	33	16	–	19
Zn	–	–	–	67	–	–	–	–	90	80	54	–	106
Ga	–	–	–	21	–	–	–	–	21	21	20	–	28
Ge	–	–	–	2	–	–	–	–	2	2	2	–	2
Rb	–	–	–	268	–	–	–	340	209	204	194	–	228
Sr	104	93	111	92	109	95	94	40	89	102	101	128	141
Y	43	38	34	32	33	36	41	8	35	34	28	35	38
Zr	187	205	189	196	198	223	213	37	197	216	180	223	220
Nb	–	–	–	15	–	–	–	9	18	17	15	–	16
Sn	–	–	–	6	–	–	–	–	4	4	4	–	5
Sb	–	–	–	0	–	–	–	–	1	1	1	–	0
Cs	–	–	–	16	–	–	–	–	22	12	17	–	14
Ba	280	365	546	453	593	333	440	85	328	365	420	392	507
Hf	–	–	–	6	–	–	–	2	6	6	6	–	6
Ta	–	–	–	2	–	–	–	–	2	1	2	–	2
W	–	–	–	196	–	–	–	–	183	148	150	–	178
Tl	–	–	–	1	–	–	–	–	2	2	2	–	1
Pb	–	–	–	32	–	–	–	–	17	21	19	–	32
Bi	–	–	–	1	–	–	–	–	6	0	1	–	1
Th	–	–	–	14	–	–	–	6	16	16	13	–	19
U	–	–	–	3	–	–	–	3	2	2	2	–	2
Sc	–	9	9	8	9	10	10	–	11	13	12	13	12
Be	–	2	2	2	2	3	2	–	2	2	3	2	

Lithology				Gabbro	Enclaves			CPC Dykes			Cretacic Dykes		
								Aplites		Mzdte	Gabbro	Tephr	Traq-Bas
Sample	CO-18	CO1-1*	CO1-12*	CO-15	CB-4e	CB-11a	CB-11b	CB-21a	CO-10	CB-24c	CB-24a	CB-24b	CO-12
SiO_2	67.73	68.39	67.81	52.56	54.04	49.86	62.30	74.75	76.76	61.98	48.07	41.42	44.68
TiO_2	0.67	0.73	0.72	0.54	0.75	0.92	0.93	0.13	0.07	0.99	2.64	2.61	2.44
Al_2O_3	15.17	15.03	15.36	16.11	20.89	23.50	14.46	14.58	13.37	21.66	16.02	14.82	17.07

(*continued on next page*)

Table 1 (*continued*)

Lithology				Gabbro	Enclaves			CPC Dykes			Cretacic Dykes		
								Aplites		Mzdte	Gabbro	Tephr	Traq-Bas
Sample	CO-18	CO1-1*	CO1-12*	CO-15	CB-4e	CB-11a	CB-11b	CB-21a	CO-10	CB-24c	CB-24a	CB-24b	CO-12
Fe_2O_3	5.04	5.46	5.45	8.50	7.08	7.32	9.02	1.19	0.74	0.47	10.91	12.41	10.48
MnO	0.07	0.10	0.07	0.14	0.08	0.09	0.14	0.03	0.01	0.01	0.17	0.14	0.23
MgO	2.19	2.17	2.30	7.69	2.47	2.56	3.58	0.35	0.17	1.21	6.53	6.01	3.81
CaO	1.75	1.51	2.05	8.45	0.64	1.08	2.04	0.47	0.52	5.11	8.67	7.50	8.51
Na_2O	2.77	2.40	2.48	2.94	1.84	1.55	1.87	3.81	3.69	7.16	3.02	2.29	3.33
K_2O	3.36	3.56	2.97	0.90	8.22	8.36	4.14	3.71	4.20	0.14	1.44	3.79	2.12
P_2O_5	0.19	0.17	0.16	0.08	0.09	0.18	0.25	0.26	0.21	0.27	0.45	0.68	0.82
LOI	1.23	1.04	1.24	1.68	2.34	3.17	1.55	0.83	0.38	0.73	1.82	7.95	5.30
Total	100.18	100.55	100.62	99.59	98.44	98.59	100.29	100.12	100.12	99.73	99.74	99.62	98.79
Q	32.28	34.83	34.66	5.54	7.07	3.22	26.57	37.59	38.45	7.81	1.01		
C	4.25	4.90	4.73		8.02	10.37	3.79	4.07	2.31	1.09			
Or	19.86	21.06	17.56	5.32	48.58	49.41	24.47	21.93	24.82	0.83	8.51	22.40	12.53
Ab	23.44	20.29	20.97	24.87	15.57	13.11	15.82	32.24	31.22	60.58	25.55	19.38	28.17
An	7.44	6.35	9.11	28.11	2.59	4.18	8.49	0.63	1.21	23.59	25.91	18.97	25.37
Di				9.33							4.38	4.12	3.02
Hy	5.45	5.39	5.73	14.83	6.15	6.38	8.92	0.87	0.42	3.01	14.23		1.66
Ol												9.15	4.51
Hm	5.04	5.46	5.45	8.50	7.08	7.32	9.02	1.19	0.74	0.47	10.91	12.41	10.48
Il	0.16	0.20	0.16	0.30	0.17	0.19	0.30	0.07	0.03	0.03	0.36	0.31	0.49
Tn				0.92							6.02		5.36
Pf												4.16	
Ru	0.59	0.63	0.64		0.66	0.82	0.78	0.09	0.06	0.97			
Ap	0.45	0.41	0.39	0.19	0.21	0.43	0.59	0.62	0.50	0.64	1.07	1.61	1.94
Total	98.96	99.52	99.40	97.91	96.10	95.43	98.75	99.30	99.76	99.02	97.95	92.51	93.53
V	86	–	–	162	127	147	136	26	7	88	283	170	190
Cr	38	71	70	289	94	115	–	nd	nd	71	107	140	–
Co	30	29	28	43	19	20	–	34	31	18	46	46	–
Ni	Nd	24	27	136	22	nd	–	nd	nd	28	105	147	–
Cu	15	–	–	32	26	14	–	nd	nd	nd	25	37	–
Zn	41	–	–	71	114	154	–	47	53	nd	101	172	–
Ga	21	–	–	18	32	46	–	23	22	23	24	25	–
Ge	2	–	–	1	2	2	–	4	3	3	2	2	–
Rb	230	149	109	84	488	557	–	316	253	7	93	142	–
Sr	108	111	192	210	68	59	85	28	64	1240	502	707	1041
Y	36	31	36	17	17	29	29	8	6	49	30	25	22
Zr	214	179	189	59	135	196	140	54	33	313	226	272	136
Nb	21	15	15	2	14	25	–	27	17	27	41	76	–
Sn	5	–	–	2	8	15	–	6	5	3	2	2	–
Sb	1	–	–	1	0	0	–	6	0	6	3	1	–
Cs	14	–	–	4	40	47	–	19	16	1	5	10	–
Ba	393	440	480	90	922	525	210	72	196	118	230	991	686
Hf	6	5	5	2	4	6	–	3	1	9	6	6	–
Ta	2	–	–	0	1	2	–	8	8	2	3	5	–
W	171	–	–	36	36	35	–	252	207	116	55	17	–
Tl	2	–	–	1	4	3	–	2	1	0	1	2	–
Pb	15	–	–	11	20	17	–	23	18	15	15	22	–
Bi	0	–	–	1	1	3	–	399	17	0	2	1	–
Th	16	12	13	2	18	25	–	4	4	22	4	6	–
U	2	Nd	nd	1	1	3	–	3	3	3	1	1	–
Sc	13	–	–	34	6	17	29	8	4	16	29	15	15
Be	2	–	–	1	6	6	2	nd	1	6	1	3	1

Major elements (wt%), CIPW norm and trace elements (ppm). Activation laboratories LTD (Canada) by ICP-MAS. (*) XRF Laboratory. Jujuy National University (Argentine). (**) XRF Laboratory. Salta National University (Argentine). nd, Not detected. –, Not analyzed.

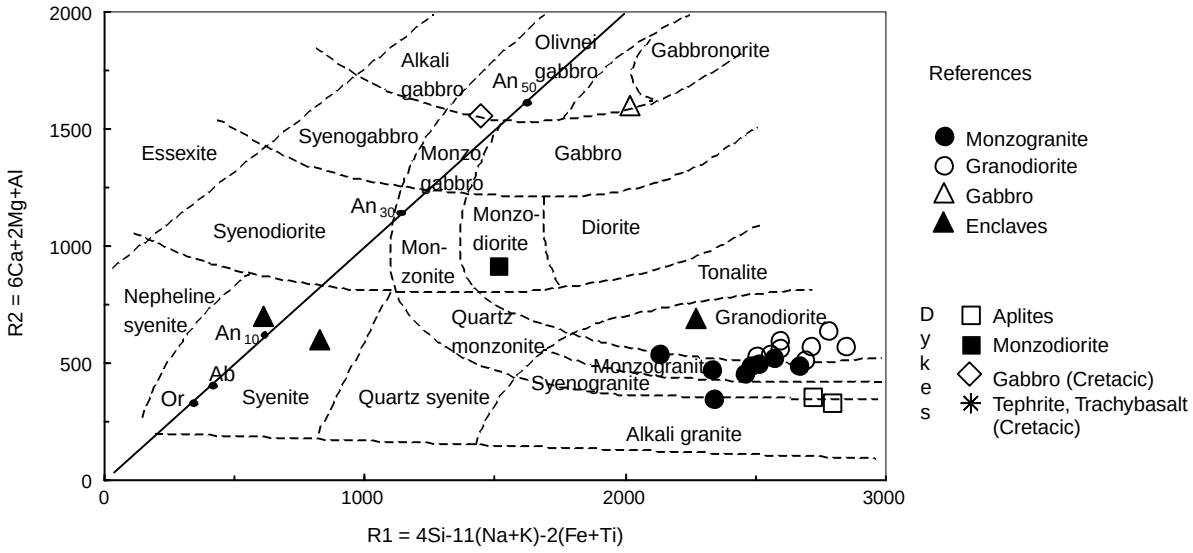

Fig. 4. Classification of CPC rocks using the parameters R1 and R2 (De la Roche et al., 1980), calculated from millication proportions.

this field due to its high Al_2O_3 and minimum K_2O content. Similarly, the analyzed rocks (except for gabbroic dikes) have an A/CNK > 1.1, the limit for I-S-type granites according to Chappell and White's (1992) classification. This value suggests fusion of sedimentary rocks as the granite origin.

The CPC samples follow a typical calc–alkaline trend, with a significant gap between the main facies and the aplitic rocks at the end of the differentiation in the AFM diagram (Fig. 7).

The Harker diagrams (Fig. 8) show that the CPC granitoids have a variation trend that could be associated with a fractionated crystallization process with 62–77 weight percent SiO_2 concentration range.

Two enclaves (CB-4e, CB-11a) with anomalous Al_2O_3 and K_2O content were not considered during the analysis of the fractional crystallization processes. The enclave CB-11b is considered the primitif member.

A negative correlation is shown among SiO_2 and TiO_2, Fe_2O_3, MnO, MgO, and CaO concentrations from CB-11b, the granodiorites, the monzogranites, and the aplites; in contrast, the Na_2O concentrations show a positive correlation among the lithologies.

Correlation among SiO_2 and trace elements is negative for Ba and Th and positive for Rb. According to Pearce et al. (1984), high values of Th and Zr indicate participation of the continental crust in the genesis of these magmas. Y and Zr show a similar tendency, with maximum concentrations in the granodiorites and monzogranites, higher than in the mafic enclave, and conspicuous diminution in the aplites, which may be interpreted as the result of zircon and monacite crystallization in the main facies. The monzodioritic dike has maximum Y, Zr, and Th values and the lowest Rb and K, which confers on it particular characteristics that set it aside from both the basic dikes and the granitoids in the CPC.

3.5.2. Rare earth elements

Table 2 shows the results obtained from 11 analyzed samples normalized to chondrite (Sun and McDonough,

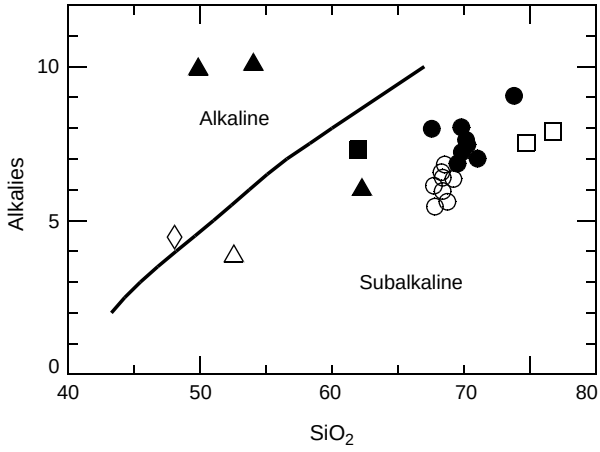

Fig. 5. SiO_2 versus $Na_2O + K_2O$ (wt%) (Irvine and Baragar, 1971). Symbols as in Fig. 4.

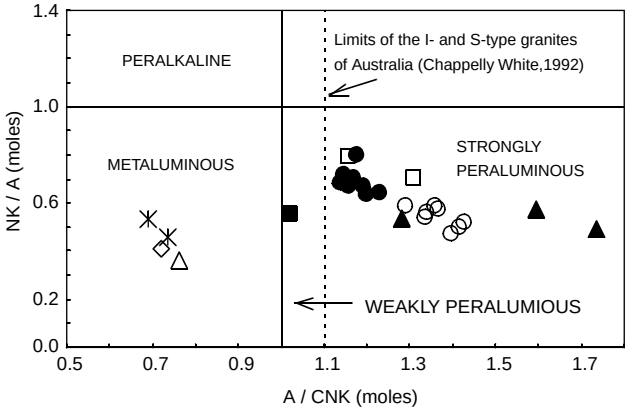

Fig. 6. Plots of $Al_2O_3/(Na_2O + K_2O)$ versus $Al_2O_3/(CaO + Na_2O + K_2O)$ (Shand, 1927). Symbols as in Fig. 4.

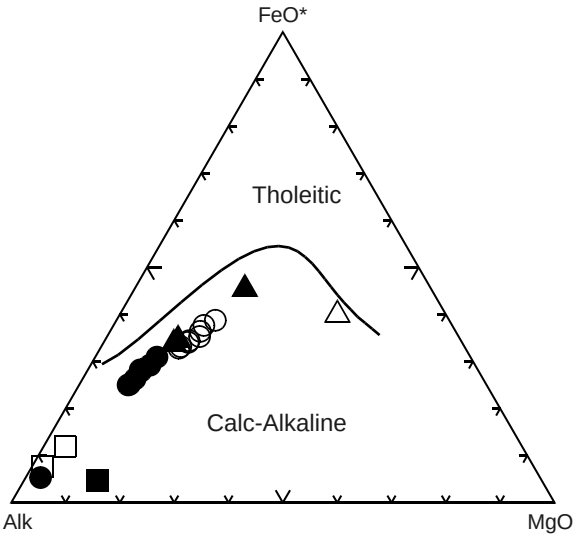

Fig. 7. AFM diagram showing calc–alkaline and tholeitic fields (Irvine and Baragar, 1971). Symbols as in Fig. 4.

1989). The same relative concentration pattern is observed for monzogranites, granodiorites, enclaves, aplites, and the monzodioritic dike (Fig. 9a), though REE concentrations in aplite are depleted nearly 10 times as much as the other rocks. These granitoids are enriched in LREE with respect to HREE, as is shown in Fig. 9(a) and Table 2 in the ΣLREE versus ΣHREE ratio, similar to the characteristic pattern of upper crust rocks.

The enclaves, granodiorites, monzogranites, aplites, and monzodioritic dike have a negative Eu anomaly (Eu/Eu* = 0.45–0.65); the monzodioritic dike is the richest in REEt, concentrated in allanite, zircon, apatite, and titanite. Fig. 9(a) shows a gradual decrease in REEt content, from the less evolved enclaves and monzodioritic dike to the intermediate granodiorite and monzogranite and on to the most evolved aplite. This progression is related to the presence of such minerals as biotite, zircon, apatite, and monacite, which—with the exception of biotite—are absent in the aplites.

The flat REE pattern of the gabbro, apparently mingled with the granodiorite (CO-15) (Fig. 9(b)), indicates a mantle source. Mingling of magmas with mantle (gabbro) and felsic crust (granodiorite) sources must be considered, but as mentioned previously, available outcrops recording this phenomenon are not sufficient for detailed studies. The samples with positive Eu anomalies (1.10–1.12, Table 2) correspond to a gabbro (CB24a) and a tephrite (Cb24b) attributed to Cretaceous magmatism. These rocks are rich in calcic plagioclase, which may concentrate Eu^{2+}. When magma has a low oxidation state, Eu^{2+} is present and can substitute (diadochic) Ca^{2+} in plagioclase (Brownlow, 1996). The tephrite is depressed in HREE and has a maximum La/Yb ratio, which suggests scarce partial melting in a cortical source.

3.6. Tectonic setting

The tectonic discrimination diagrams employed in previous studies of Paleozoic magmatism have led to a broad range of interpretations (e.g. Coira et al., 1999). In this case, several graphs were used to discriminate the tectonic setting using geochemical data. Diagram R1–R2 (Fig. 10) is the only one that permits a clear classification and places the analyzed granitoids in the syncollisional granite field. The enclave dispersion in the graph is applicable only to granite rocks *sensu stricto*. A tectonic classification was not possible using Pearce et al.'s (1984) diagram (Fig. 11), because the samples plot within the limits of different tectonic fields.

4. Discussion

The southern portion of the Cobres Range shows a more complex picture than previously supposed, with two well-defined plutons, a granodiorite, and a monzogranite pluton that form part of the CPC. These plutons show differences in texture, composition, and deformation intensity.

The remarkable differences in the structural analyses are as follows: The granodiorite registers heterogeneous deformation, varying from portions with a solid-state deformational fabric practically imperceptible to the naked eye to high deformation bands up to hundreds of meters thick with very well-defined foliation and lineation. The granodiorite and country rock deformational fabrics originated at medium to high temperature, as discussed in Section 3.1.

In contrast, the monzogranite is only affected by thin deformation zones, which, according to the chlorite that partially defines the foliation, occurred at low temperature. These strips are generally related to aplite and quartz dikes, so nucleation of the deformation may have been enhanced by fluid activity and rheological variations.

The differences in deformational fabrics mentioned for the granodiorite and monzogranite highlight their clear separation as mutually unrelated phenomena in geological history. However, cartographic–structural and geochemical–petrological analyses of the plutons and country rock suggest they are part of a single history and directly related. In this context, a geochemical–petrological investigation offers information consistent with the hypothesis that these two plutons derive from one magmatic source, specifically: (1) the similarity in their mineral accessories (biotite, tourmaline, apatite, zircon, monacite), (2) their strong peraluminousity, (3) their correspondence to the same calc–alkaline series, (4) the lineal distribution of the rocks in the Harker type diagrams that shows continuous evolution, and (5) the similar REE patterns in both petrotypes.

Furthermore, the structural data indicate that the granodiorite emplacement, metamorphic zoning from spotted phyllite to gneiss at the contact area, and mid- to high-temperature deformation are contemporary events related to a thermal anomaly. The attitude of foliation, especially in the metamorphic rock, lineation, and distribution of the metamorphic rock grades (Fig. 2), clearly show that the high-temperature deformation had an extensional component in a NE to E direction.

The tectonic discrimination diagrams based on the CPC geochemical data do not permit a clear interpretation but raise the possibility of various scenarios in line with those of other

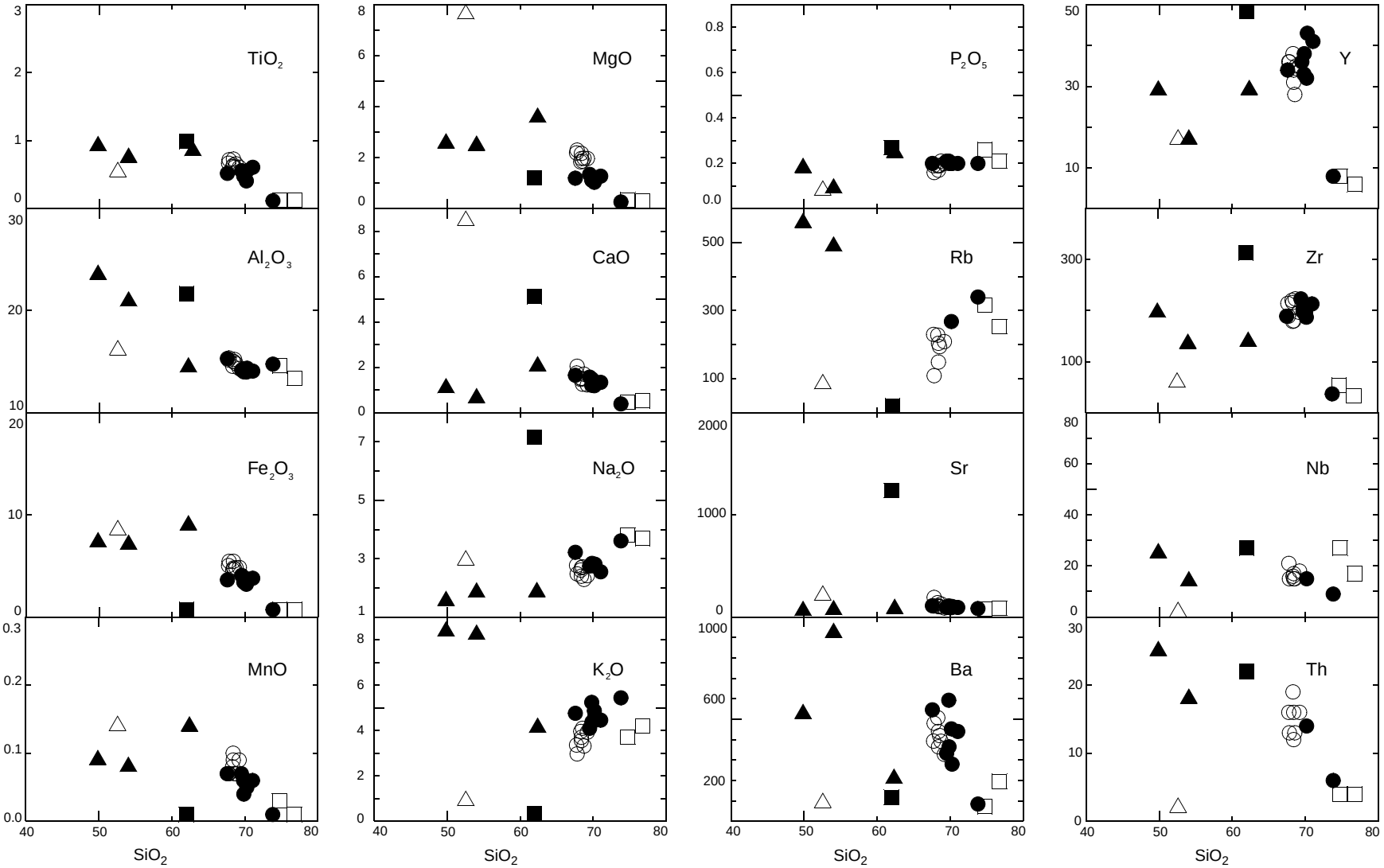

Fig. 8. Harker variation diagrams for the CPC rocks. Major and trace elements (wt% and ppm, respectively). Symbols as in Fig. 4.

Table 2
Analytical data of rare earth elements (ppm)

Lithology	MzGte	Grano-diorites			Gabbro	Enclave	CPC Dykes		Cretacic Dyke		
							Aplites		Mzdte	Gabbro	Teph
Sample	CO-8	CB-22	CB-37	CO-18	CO-15	CB-11a	CB-21a	CO-10	CB-24c	CB-24a	CB-24b
La	30.82	42.76	35.65	38.67	4.00	55.34	6.73	4.69	53.46	31.02	55.07
Ce	65.36	88.77	72.39	80.63	9.38	107.46	14.65	9.61	113.69	66.24	106.44
Pr	7.15	9.72	8.36	8.71	1.22	12.60	1.75	1.05	12.93	7.69	11.27
Nd	28.73	37.56	32.05	33.30	5.96	50.38	6.70	3.86	49.86	32.47	44.29
Sm	6.18	7.63	6.63	7.10	1.84	9.73	1.73	0.94	10.42	7.19	8.39
Eu	1.06	1.29	1.24	1.20	0.67	1.61	0.23	0.19	1.91	2.52	2.83
Gd	5.52	6.80	5.74	6.31	2.33	8.00	1.38	0.81	9.33	6.74	7.17
Tb	1.05	1.10	0.97	1.10	0.48	1.22	0.27	0.17	1.56	1.06	0.99
Dy	6.14	6.87	5.81	7.11	3.08	6.11	1.62	1.04	9.68	6.37	5.59
Ho	1.19	1.31	1.09	1.33	0.64	1.09	0.27	0.20	1.82	1.15	0.94
Er	3.69	3.89	3.25	3.97	1.98	3.14	0.80	0.65	5.21	3.25	2.53
Tm	0.54	0.61	0.48	0.64	0.29	0.44	0.15	0.12	0.77	0.44	0.32
Yb	3.52	3.66	3.01	3.80	1.97	2.76	1.08	0.91	4.85	2.72	1.97
Lu	0.51	0.53	0.44	0.51	0.30	0.41	0.15	0.13	0.65	0.40	0.27
REE	161.45	212.52	177.13	194.37	34.13	260.29	37.51	24.37	276.15	169.25	248.07
LREE	138.24	186.45	155.09	168.40	22.39	235.51	31.56	20.15	240.35	144.61	225.47
HREE	22.16	24.78	20.79	24.77	11.07	23.17	5.72	4.04	33.89	22.12	19.77
La/Yb	5.91	7.87	7.98	6.86	1.37	13.50	4.20	3.46	7.43	7.68	18.84
La/Sm	3.14	3.53	3.38	3.42	1.37	3.58	2.45	3.14	3.23	2.71	4.13
Gd/Yb	1.27	1.50	1.54	1.34	0.95	2.34	1.03	0.72	1.55	2.00	2.93
Eu/Eu*	0.55	0.55	0.62	0.55	0.99	0.56	0.45	0.65	0.59	1.10	1.12

Activation laboratories LTD (Canada) by ICP-MAS.

authors (Bahlburg and Hervé, 1997; Coira et al., 1999; Coira and Koukharsky, 2002). Batchelor and Bowden's (1985) diagram (Fig. 10) delineates a collisional tectonic setting for these rocks. However, there is no evidence, either local (deformation, metamorphism) or regional (stratigraphy, Bahlburg, 1990; Moya, 1999; Benedetto et al., 2002; magmatism, Coira et al., 1999; Coira and Koukharsky, 2002; metamorphism, Lucassen et al., 1999), consistent with the geotectonic setting.

Transpressive (Hongn and Mon, 1999) and transtensive (Coira et al., 1999) models developed in continental crust have been proposed for the origin, emplacement, and deformation of the eastern Puna Lower Paleozoic magmatism. Available data for the southern portion of the Cobres Range fit these models, whose kinematics show oblique components. In this sense, the CPC would be part of a deformational history that began with the folding of the Ordovician succession under lower greenschist metamorphic conditions. Fold axial lines plunging at high angle suggest a horizontal movement component during folding; consequently, formation of dilatational bends can be expected during this stage.

A thermal anomaly occurred during this period, promoting the generation of magmas, origin of metamorphic rocks (spotted rocks, schist, gneiss), formation of high-temperature deformation zones, and emplacement and deformation of the granodiorite. Changes in deformation conditions (attenuation of thermal anomaly and/or increase in deformation rates) lead to fracture formation at different scales; these fractures are perpendicular to the extension direction indicated by stretching lineation. Such structures control the emplacement of the

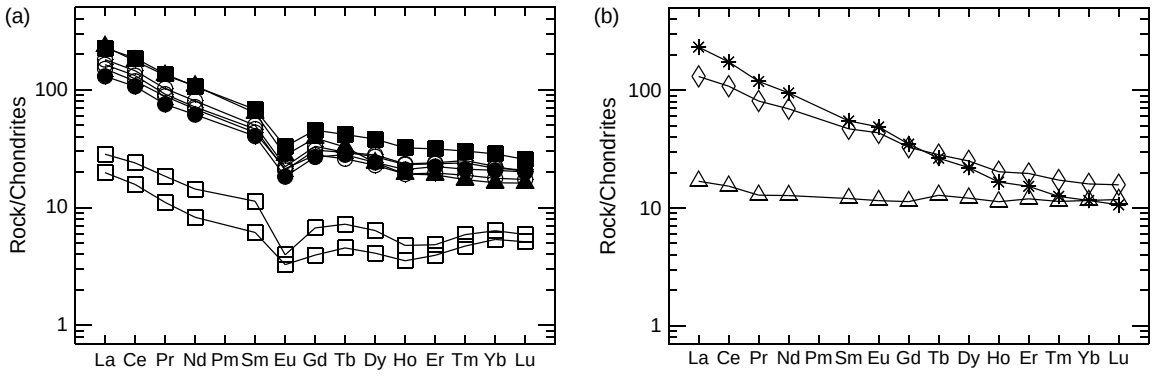

Fig. 9. REE diagrams for (a) CPC rocks and (b) basic dikes; values normalized to chondrite of Sun and McDonough (1989). Symbols as in Fig. 4.

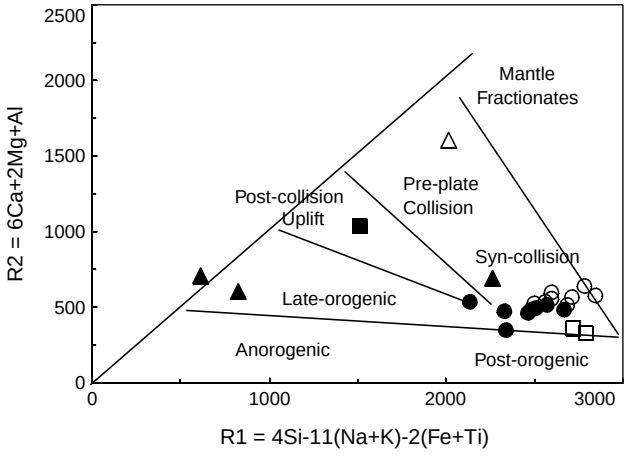

Fig. 10. Tectonic discrimination diagram using the parameters R1 and R2 (Batchelor and Bowden, 1985), calculated from millication proportions. Symbols as in Fig. 4.

monzogranite and dikes. In this context, the different chemical signatures offered by the CPC would respond to magmas generated in the crust (felsic magma chambers with minor participation of gabbros). Gabbros with mantle signatures suggest the ascent of deep magmas during the extensional stages registered in the granodiorite, especially in its country rock. The process, which involves crust recycling, coincides with similar proposals for most of the Paleozoic plutons in the basement of the northern Argentine and Chilean regions (Damm et al., 1990; Coira and Koukharsky, 2002) and explains the extremely varied results in the diagrams usually employed to determine tectonic settings.

The mingling of basic and acidic magmas, as described in nearby areas (Pérez and Coira, 1999) and suggested in this contribution, continues to be researched. Future studies will focus on the northern portion of the range, which is composed almost totally of granodiorites; because gabbros are always related to granodiorites, the possibility of finding new outcrops that record the process is greater. The CPC is syntectonic, and its plutons were emplaced in different stages of the tectomagmatic history of approximately 476 Ma ago (Lork and Bahlburg, 1993), which holds special interest for analyzing the evolution of the Ordovician basins because it indicates the presence of a tectonometamorphic episode in the Lower Arenigian overprinting the cleavage related to the folding of the Ordovician successions. It constitutes new evidence in favor of intra-Ordovician deformations (Bahlburg, 1990; Moya, 1999; Hongn and Mon, 1999). In addition, the Upper Ordovician deposits are affected by folding and related cleavage (Hongn and Mon, 1999), consistent with the hypothesis of alternate extension and contraction periods during the Lower Paleozoic in the Puna. Collins (2002) names extensional accretionary orogens those that evolved in backarc settings and register a history dominated by periods of extension with short periods (approximately 10 Ma years) of contraction. This alternation relates to the kinematics of the subducted plate that originated the arc. In this model, extensional periods produce thermal anomalies that generate felsic magmas by melting of the continental crust and ascent of mantle-related basic rocks.

Genesis of the CPC rocks can be explained this way because it best fits the available local and regional data. First, there is a Lower Paleozoic arc in the western Puna that evolved from the Upper Cambrian to the Mid Ordovician (Bahlburg and Hervé, 1997; Coira et al., 1999; Coira and Koukharsky, 2002; Zimmermann and Bahlburg, 2003). Second, the Cambrian and Lower Ordovician basins of the Eastern Cordillera and Puna are extension related (Bahlburg, 1990; Moya, 1999). Third, basic rocks with a clear extensional setting geochemical signature intercalate with the Ordovician deposits of Cochinoca (Coira et al., 1999) and Aguilar (Coira and Darren, 2002) ranges. One gabbro (CO-15) from the Cobres Range shows geochemical signatures suggesting a mantle source. Fourth, a

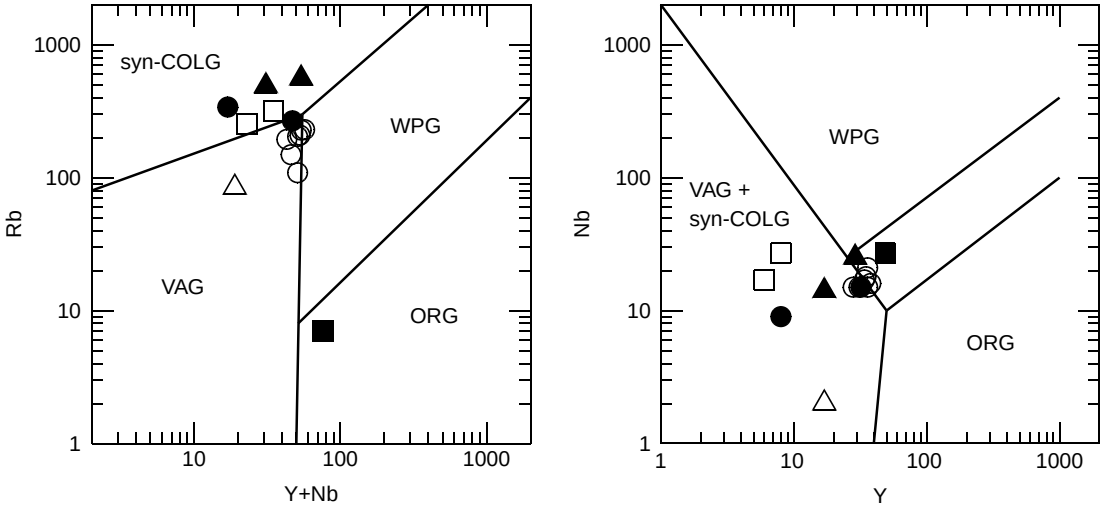

Fig. 11. Tectonic discriminant diagram (Pearce et al., 1984). Concentrations in ppm. Symbols as in Fig. 4. ORG, ocean ridge granites; VAG, volcanic arc granites; syn-COLG, syn-collision granites; WPG, within-plate granites.

protracted thermal anomaly occurred during the Early Paleozoic (Lucassen and Becchio, 2003). Fifth, the geochemistry of the CPC plutons points to continental crust fusion as a magmatic source. Sixth, structural analysis indicates the alternation of extension and contraction events during the Tremadocian and Arenigian.

5. Conclusions

The petrological–geochemical and cartographic–structural analyses of the southern Cobres Range indicate that the CPC is formed by two main plutons, a granodiorite and a monzogranite, and small bodies of gabbros, acidic dikes, and episyenite strips. These rocks are part of a continuous tectomagmatic evolution occurring approximately 476 Ma ago, the age of monazite crystallization in the granodiorite (Lork and Bahlburg, 1993). The CPC is syntectonic, though the granodiorite and monzogranite plutons represent different stages in the tectomagmatic history.

Their mineralogy and geochemistry suggest the comagmatic character of the granodioritic and monzogranitic plutons. They are subalkaline, strongly peraluminous, and follow a typical calc–alkaline trend with a significant gap between the principal facies and aplites. The Harker diagrams show, for the CPC granitoids, a variation trend that could be associated with a fractionated crystallization process, which begins with the enclaves, continues with granodiorites and monzogranites, and ends with the aplites.

The REE patterns are similar for enclaves, granodiorites, monzogranites, aplites, and acidic dikes, though the aplites record depleted concentrations. Their distribution, together with those from the other trace elements, corresponds to that of rocks originated from the continental crust. Gabbros included in the CPC show a geochemical signature compatible with mantle filiations. In turn, this signature separates them from other basic rocks that should be related to Cretaceous magmatism.

Discrimination of the tectonic setting in which the granites originated is not clear, because the plutons are of cortical origin, which implies crust-recycling phenomena. The hypothesis that best integrates the available data—thermal anomaly, alternation of deformation phases with extension and contraction components, magmatic rocks with a greater volume of cortical origin, and smaller volume of mantle filiation—relates the CPC with an extensional accretionary orogen, according to Collins (2002).

Acknowledgements

This work was supported by the Agencia Nacional de Promoción Científica y Tecnológica (PICT 2302 and 07-08724) and Consejo de Investigaciones de la Universidad Nacional de Salta (N° 1234). Instituto de Geología y Minería (UNJu) and Secretaría de Minería y Recursos Energéticos (Salta) gave logistic support for fieldwork. The manuscript was much improved after a revision by Beatriz Coira and two anonymous reviewers. Mario Valdez is sincerely acknowledged for improving the final English version of the manuscript.

References

Acuña, P.A., unpublished. Estructura paleozoica del tramo austral de la sierra de Cobres. Universidad Nacional de Salta, Facultad de Ciencias Naturales, Tesis Profesional, 152p.

Bahlburg, H., 1990. The Ordovician basin in the Puna of NW Argentina and N Chile: Geodynamic evolution from back-arc to foreland basin. Geotektonische Forschungen, Stuttgart 75, 1–107.

Bahlburg, H., Hervé, F., 1997. Geodynamic evolution and tectonostratigraphic terranes of northwestern Argentina and northern Chile. Geological Society of America Bulletin 109, 869–884.

Batchelor, R.A., Bowden, P., 1985. Petrogenetic interpretation of granitoid rock series using multicationic parameters. Chemical Geology 48, 43–55.

Benedetto, J.L., Brusa, E.D., Pompei, J.F., 2002. El Ordovícico de la región de Susques-Huancar (Puna Oriental de Jujuy): Precisiones sobre su edad y significado estratigráfico. 15 Congreso Geológico Argentino, El Calafate, Actas 1, 572–577.

Brownlow, A.H., 1996. Geochemistry, second ed. Prentice Hall, New Jersey. 580 pp.

Chappell, B.W., White, A.J.R., 1992. I- and S-type granites in the Lachlan Fold Belt. Transactions of the Royal Society of Edinburgh, Earth Sciences 83, 126.

Coira, B., Darren, J., 2002. Magmatismo ultrabásico-básico alcalino sin-extensional arenigiano en el flanco sudoccidental de la sierra de Aguilar, provincia de Jujuy. 15 Congreso Geológico Argentino, El Calafate, Actas 1, 122–127.

Coira, B., Koukharsky, M., 2002. Ordovicician volcanic activity en the Puna, Argentina. In: Aceñolaza, F.G. (Ed.), Aspects of the Ordovician System in Argentina Serie de Correlación Geológica, vol. 16. INSUGEO, Tucumán, pp. 267–280.

Coira, B., Davidson, J., Mpodozis, C., Ramos, V., 1982. Tectonic and magmatic evolution of the Andes northern Argentina and Chile. Earth Science Reviews 18, 303–332.

Coira, B., Kay, S., Mahlburg, P.B., Woll, B., Hanning, M., Flores, P., 1999. Magmatic sources and tectonic setting of Gondwana margin Ordovician magmas, northern Puna of Argentina and Chile. In: Ramos, V.A., Keppie, J.D. (Eds.), Laurentia-Gondwana Connections before Pangea. Geological Society of America Special Paper 336, Boulder, Colorado, pp. 1–26.

Collins, W.J., 2002. Nature of extensional accretionary orogens. Tectonics 21 (4), 6.1–6.11.

Damm, K.W., Pichowiak, S., Harmon, R.S., Todt, W., Kelley, S., Omarini, R., Niemeyer, H., 1990. Pre-Mesozoic evolution of the Central Andes: the basement revisited. In: Kay, S.M., Rapela, C.W. (Eds.), Plutonism from Antartica to Alaska. Geological Society of America Special Paper 241, Boulder, Colorado, pp. 101–126.

De la Roche, H., Leterrier, J., Grandclaude, P., Marchal, M., 1980. A classification of volcanic and plutonic rocks using R1R2 diagram and major-element analyses—its relationships with current nomenclature. Chemical Geology 29, 183–210.

Hongn, F.D., 1994. Estructuras precámbricas y paleozoicas del basamento del borde oriental de la Puna; su aplicación para el análisis regional de la faja eruptiva. Asociación Geológica Argentina Revista 49 (3–4), 256–268.

Hongn, F.D., Mon, R., 1999. La deformación ordovícica en el borde oriental de la Puna. En González Bonorino, G., Omarini, R., Viramonte, J.G. (Eds.), Geología del Noroeste Argentino. Relatorio 14° Congreso Geológico Argentino, Salta, 1, pp. 212–216.

Hongn, F., Acuña, P., Mon, R., Kirschbaum, A., 2001. Deformación paleozoica en el área de La Colorada. Sierra de Cobres (NO de la Argentina). VII Congreso Argentino de Geología Económica, Salta, Actas 1, pp. 65–71.

Irvine, T.N., Baragar, W.R., 1971. A guide to the chemical classification of the common volcanic rocks. Canadian Journal of Earth Sciences 8, 523–548.

Lira, R., Kirschbaum, A., 1990. Geochemical evolution of granites from the achala batholith of the sierras pampeanas, Argentina. In: Kay, S.M.,

Rapela, C.W. (Eds.), Plutonism from Antartica to Alaska. Geological Society of America Special Paper 241, Boulder, Colorado, pp. 67–76.

Lork, A., Bahlburg, H., 1993. Precise U-Pb ages of monazites from the faja eruptiva de la Puna oriental, and the Cordillera Oriental, NW Argentina. Actas 12° Congreso Geológico Argentino y 2° Congreso de Exploración de Hidrocarburos, Mendoza 4, 1–6.

Lucassen, F., Becchio, R., 2003. Timing of high-grade metamorphism: early Paleozoic U-Pb formation ages of titanite indicate long-standing high-T conditions at the western margin of Gondwana (Argentina, 26°-29°S). Journal of Metamorphic Geology 21, 649–662.

Lucassen, F., Franz, G., Thirlwall, M.F., Mezger, K., 1999. Crustal recycling of metamorphic basement: late Paleozoic granitoids of northern Chile (∼22°S). Implications for the composition of the andean crust. Journal of Petrology 40 (10), 1527–1551.

Lurgo Mayón, C., Segal, S., Zappettini, E., 1999. El yacimiento de sulfuros masivos La Colorada, Salta. In: Zappettini, E. (Ed.), Recursos Minerales de la República Argentina, vol. 35. Instituto de Geología y Recursos Minerales. SEGEMAR, Buenos Aires, Anales, pp. 487–492.

Méndez, V., Navarini, A., Plaza, D., Viera, V., 1973. Faja eruptiva de la Puna oriental. Actas 5° Congreso Geológico Argentino, Córdoba 4, 89–100.

Menegatti, N., 2001. El Complejo alcalino Sierra de Rangel, Provincia de Salta, República Argentina. (Inéd.). Universidad Nacional de Salta, Facultad de Ciencias Naturales. Tesis Doctoral, 157 pp.

Moya, M.C., 1999. El Ordovícico de los Andes del Norte Argentino. En González Bonorino, G., Omarini, R., Viramonte, J., (Eds.), Geología del Noroeste Argentino. Relatorio 14° Congreso Geológico Argentino, Salta, 1, pp. 134–152.

Passchier;, C., Trouw, R., 1996. Microtectonics. Springer, Berlin (289pp.).

Pearce, J.A., Harris, B.W., Tindle, A.G., 1984. Trace element discrimination diagrams for the tectonic interpretation of granitic rocks. Journal of Petrology 25 (4), 956–983.

Pérez, B., Coira, B., 1999. El granito de la Sierra de Tanque, borde oriental de la Puna Jujeña. Actas XIV Congreso Geológico Argentino, II, 159–162.

Rapela, C.W., Pankhurst, R.J., Casquet, C., Baldo, E., Saavedra, J., Galindo, C., Fanning, C.M., 1998. The Pampean Orogeny of the southern proto-Andes: Cambrian continental collision in the Sierras de Córdoba.. In: Pankhurst, R.J., Rapela, C.W. (Eds.), The Proto-Andean Margin of Gondwana. Geological Society, Special Publications 142, London, pp. 181–217.

Shand, S.J., 1927. Eruptive Rocks. Wiley, New York.

Sun, S.S., McDonough, W.F., 1989. Chemical ans isotopic systematics of aceanic basalts: implications for mantle compositions. In: Saunders, A.D., Norry, M.J. (Eds.), Magmatism in the Ocean Basins, vol. 42. Special Publications of the Geological Society of London, London, pp. 313–345.

Vaccari, E., Martínez, M., Hongn, F.D., 1999. Trilobites tremadocianos de la Formación Taique en la quebrada del río Taique, Salta, Argentina. Resúmenes 14° Congreso Geológico Argentino, Salta, pp. 53.

Zappetinni, E.O., unpublished. Geología y metalogénesis de la región comprendida entre las localidades de Santa Ana y Cobres, provincias de Jujuy y Salta, República Argentina. Universidad de Buenos Aires, Facultad de Ciencias Exactas, Tesis Doctoral, 180 pp.

Zimmermann, U., Bahlburg, H., 2003. Provenance analysis and tectonic setting of the Ordovician clastic deposits in the southern Puna basin, NW Argentina. Sedimentology 50, 1079–1104.